NRC Research Press

ARTICLE

Discrete element modeling of fluid injection–induced seismicity and activation of nearby fault[1]

Jeoung Seok Yoon, Günter Zimmermann, Arno Zang, and Ove Stephansson

Abstract: Enhanced geothermal systems, shale gas, and geological carbon sequestration all require underground fluid injection in high-pressure conditions. Fluid injection creates fractures, induces seismicity, and has the potential to reactivate nearby faults that can generate a large magnitude earthquake. Mechanisms of fluid injection–induced seismicity and fault reactivation should be better understood to be able to mitigate larger events triggered by fluid injection. This study investigates fluid injection, induced seismicity, and triggering of fault rupture using hydromechanical-coupled discrete element models. Results show that a small amount of fluid pressure perturbation can trigger fault ruptures that are critically oriented and stressed. Induced seismicity by rock failure shows in general higher *b*-values (slope of magnitude–frequency relation) compared to seismicity triggered by the fault fracture slip. Numerical results closely resemble observations from geothermal and shale-gas fields and demonstrate that discrete element modeling has the potential to be applied in the field as a tool for predicting induced seismicity prior to in situ injection.

Key words: induced seismicity, fault reactivation, large-magnitude events, triggered seismicity, magnitude–frequency relation *b*-value.

Résumé : Les systèmes géothermiques améliorés, l'extraction du gaz de schiste et la séquestration du carbone géologique nécessitent l'injection de fluides à haute pression dans le sous sol. Ce type d'injection génère des fractures, cause des secousses sismiques et peut réactiver des failles avoisinantes, lesquelles peuvent provoquer des tremblements de terre de forte magnitude. Il serait utile de mieux comprendre les mécanismes des séismes induits par l'injection de fluides et ceux de la réactivation de failles, et ce afin d'être en mesure de prévenir les événements graves causés par l'injection de fluide. Dans le présent article, on étudie l'injection de fluides, la sismicité induite et le déclenchement de ruptures de failles à l'aide de modèles couplés hydromécaniques basés sur la méthode des éléments discrets. Les résultats montrent qu'une légère perturbation de la pression du fluide injecté peut déclencher des ruptures d'orientation critique soumises à des contraintes. La sismicité induite par la rupture de roches est généralement caractérisée par des valeurs de *b* (pente de la fonction de relation entre la magnitude et la fréquence) par rapport à celles observées dans le cas de la sismicité déclenchée par le cisaillement de rupture des failles. Les résultats numériques se rapprochent beaucoup des observations faites sur les sites géothermiques ou d'extraction de gaz de schiste et montrent que la modélisation basée sur la méthode des éléments discrets pourrait être utilisée sur ces sites comme outil servant à prédire la sismicité induite avant l'injection de fluides in situ. [Traduit par la Rédaction]

Mots-clés : sismicité induite, réactivation de failles, incidents de forte magnitude, sismicité déclenchée, valeur de *b*: pente de la fonction de relation entre la magnitude et la fréquence.

Introduction

Developing an enhanced geothermal system (EGS) requires the creation of highly permeable heat exchange. This is usually achieved by hydraulic stimulation, where fluid is injected underground in high-pressure conditions to create new mode I fractures or to enhance dilation of pre-existing joints and fractures by shearing in mode II. Fluid injection can cause stress changes locally through the stress shadow effect, as well as reactivation of pre-existing joints and slip of nearby faults, which consequently can trigger larger magnitude events (LMEs), e.g., Basel EGS (Häring et al. 2008; Kraft et al. 2009; Mukuhira et al. 2013). Larger magnitude events induced in geothermal sites were collected and analyzed in Zang et al. (2014).

Presence of faults and their reactivation potential have also received increasing attention in shale gas development, due to a concern that hydraulic fractures could propagate upward through the overburden and into shallow groundwater aquifers and thereby contaminate groundwater. In most cases, such upward migration of induced seismicity has been associated with fracturing along subvertical faults associated with their reactivation, creating new flow pathways for hydrocarbon migration and potentially triggering LMEs. One such case is the Presse Hall well site in Lancashire County, near Blackpool, UK, where two seismic events of magnitude 2.3 and 1.5 were observed (de Pater and Baisch 2011).

Additionally, in geological carbon sequestration the risk of induced seismicity is of general concern because of the large-scale pressurization resulting from CO_2 injection. Induced seismicity remains a major issue for public acceptance for the operations located near active, potentially seismic faults. The possibility

Received 14 October 2014. Accepted 13 May 2015.

J.S. Yoon, G. Zimmermann, A. Zang, and O. Stephansson. Helmholtz Centre Potsdam GFZ German Research Centre for Geosciences, Telegrafenberg D 14473, Potsdam, Germany.

Corresponding author: Jeoung Seok Yoon (e-mail: jsyoon@gfz-potsdam.de; yoon_gfz@hotmail.com).

[1]This paper is part of the "Recent developments in geomechanics and geophysics" Special Issue, which is based on presentations from the 5th International Colloquium on Geomechanics and Geophysics held in Karolinka, Czech Republic, 25–27 June 2014.

Fig. 1. (*a*) Assembly of bonded particle model and pore space network and flow channels. (*b*) Distribution of fluid pressure and induced bond failures.

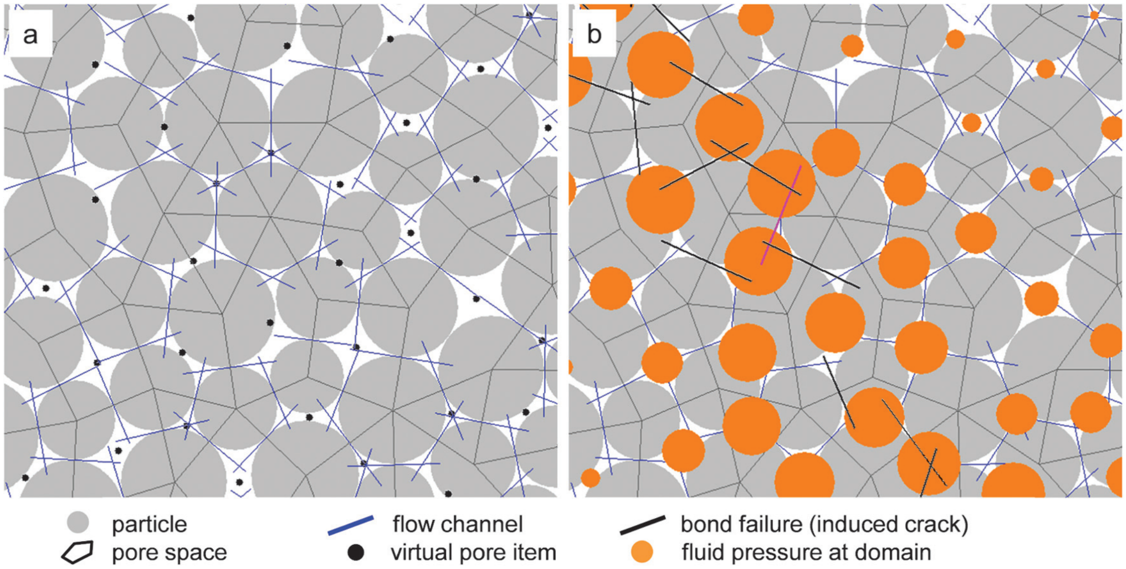

exists that such induced seismicity may also result from undetected faults (Mazzoldi et al. 2012).

In this context, it is important to understand how fluid injection affects nearby fault movement and the potential for generating LMEs. This study investigates using discrete element modeling fluid injection into a porous medium with a fault zone. Questions of how a fault zone behaves due to a nearby fluid injection and how induced and triggered seismicity are correlated with fault slip are studied. Results of this study may provide explanations for the phenomenon related to post shut-in LMEs, where injection is conducted adjacent to a fault zone oriented in a direction prone to being reactivated by the stress change.

Presented here is discrete element–based modeling of fluid injection–induced seismicity in a reservoir with an inclined fault zone. Dissimilar to recent studies by Zang et al. (2013) and Yoon et al. (2014, 2015*a*, 2015*b*), the model investigated in this study contains a large fault zone. Not only the seismic events computed from bond breakages, but also the seismic events by fracture slip are taken into account and compared with field observations. This type of modeling is of importance as several EGS operations were conducted in Europe — e.g., Basel (Häring et al. 2008; Mukuhira et al. 2013) and St. Gallen (Diehl et al. 2014) in Switzerland — where fluid injection was conducted within and at close vicinity to fault zones that are critically oriented and stressed, during which seismic occurrences with values of $M_L \geq 3$ were felt on the surface.

Hydromechanical-coupled dynamic discrete element model

A hydromechanical-coupled, fluid flow algorithm is implemented in Particle Flow Code 2D (PFC2D, ICG 2008). Flow of viscous fluid in a bonded particle assembly is modeled and fluid volume and pressure driven breakages of bonds in mode I and mode II are simulated (Hazzard et al. 2002; Zang et al. 2013; Yoon et al. 2014). Fluid flow is simulated by assuming that each bonded contact is a flow channel (Fig. 1*a*, flow channel). These channels connect pore spaces (Fig. 1*a*, pore space) where fluid volume and pressure are stored. Fluid flow, q, is driven by the pressure difference between two neighboring pore spaces and is governed by the Cubic law (eq. (1))

$$q = e^3 \Delta P_f / 12\mu L \tag{1}$$

where e is the hydraulic aperture, $\Delta P_f/L$ is the pressure gradient between two neighboring pores, L is the flow channel length (equal to the average diameter of two neighboring particles), and μ is the fluid dynamic viscosity (= 1E–3 Pa·s).

Hydraulic aperture e changes as a function of normal stress on the flow channel (particle contact), σ_n, using the equation (Hökmark et al. 2010)

$$e = e_{inf} + (e_0 - e_{inf}) \exp(-0.15\sigma_n) \tag{2}$$

where e_{inf} is the hydraulic aperture at high normal stress (= 50 μm) and e_0 is the hydraulic aperture when σ_n = 0. The e_0 is calibrated from an assumed permeability of the reservoir model, k (= 1E–12 m^2).

Fluid pressure increases per time step, Δt, in a pore space and is computed as a function of fluid bulk modulus, K_f; volume of pore space, V_d; net fluid volume in a pore space per time step, $\Sigma q \Delta t$; and volume change of pore space due to mechanical effect, ΔV_d.

The force term that is applied to the particles surrounding a pore space is a product of fluid pressure, P_f, and the surface area onto which the fluid pressure exerts. The force displaces the particles, which consequently changes the stress state at the surrounding particle contacts, which in turn changes the hydraulic aperture e, and thereby the flow volume.

Fluid injection and migration are significantly influenced by reservoir permeability. Flow channel apertures are the key parameters in this issue, which are calibrated using the bulk permeability, k, assumed for the model. Also, the hydraulic aperture is programmed to decrease with increasing normal stress on the flow channel (fracture plane), which is simulated by the nonlinear function (eq. (2)).

Each bond breakage from the pressure buildup in a pore space is a fracturing process associated with seismic energy radiation. The simulation runs in dynamic mode with a realistic level of energy attenuation in rock using the seismic quality factor Q (= 100) and S-wave velocity (= 2 km/s). When a bond breaks, part of the stored strain energy is released. Along the boundaries, a 150 m thick region is assigned with high viscous damping to minimize the reflection of the seismic wave.

The moment tensor method is used to compute the moment tensor ($\boldsymbol{M}_{ij}$) associated with bond breakages (eq. (3); Hazzard and Young 2002; Hazzard et al. 2002; Al-Busaidi et al. 2005; Zhao and

Fig. 2. (*a*) 2 km × 2 km reservoir model with a through-going fault zone subjected to maximum and minimum horizontal stresses; (*b*) representation of a fault zone by a collection of damage zones and fault core fractures; (*c*) synoptic figure of fault zone (after Munier and Hökmark 2004).

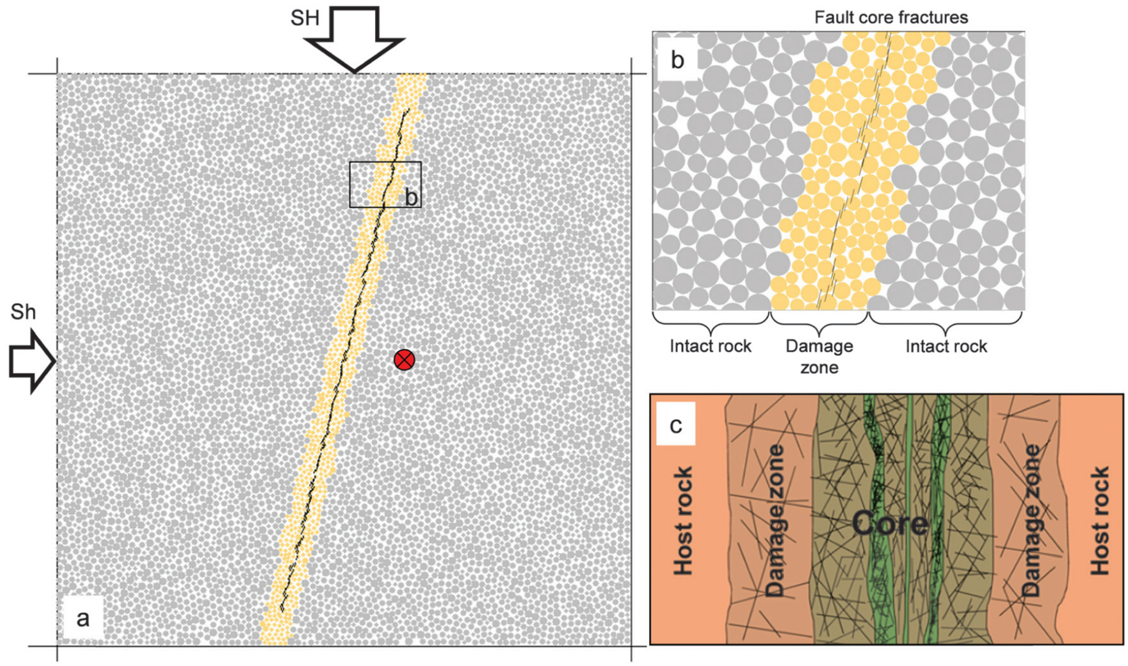

Young 2011; Yoon et al. 2012, 2013, 2014). Seismic moment M_0 is computed from the moment tensor components (eq. (4)), then converted to a moment magnitude, M_w (eq. (6)). The moment magnitude of the fault fracture slip is calculated using eq. (5) and then converted to a moment magnitude using eq. (6) (Hanks and Kanamori 1979)

(3) $\boldsymbol{M}_{ij} = \Sigma \Delta F_i R_j \quad (i = 1, 2; j = 1, 2)$

(4) $M_0 = \left[\left(\Sigma m_i^2\right)/2\right]^{0.5} \quad (i = 1, 2)$

(5) $M_0 = GAd$

(6) $M_w = (2/3)\log(M_0) - 6$

where ΔF_i is the ith component of the change in contact force, R_j is the jth component of the distance between the contact point and the event centre, m_i is the eigenvalue of the moment tensor, G is the shear modulus (= 30 GPa), A is the fracture slip area (m²), and d is the slip displacement (m).

Model description and parameters

The reservoir model is 2 km × 2 km in size (Fig. 2*a*). Diameters of the particles range between 20 and 30 m. The diameter range chosen is comparable to that used in similar studies by Hazzard et al. (2002) and Baisch et al. (2010). In Hazzard et al. (2002), fluid injection and induced seismicity in the Soultz geothermal reservoir is modeled using an average particle diameter of 19.7 m. Baisch et al. (2010) used the Block–Spring model to simulate fluid injection–induced seismicity at Soultz, with a fracture zone consisting of individual blocks, i.e., slip patches of 20 m side length.

A through-going fault zone is added in a relatively intact rock (Fig. 2*b*). According to the schematic figure in Fig. 2*c* (Munier and Hökmark 2004), the fault zone is designed with a collection of particles with smaller radii and lowered stiffness, friction, and strength at their contacts compared to the surrounding particles representing the host rock (Fig. 2*b*). Within the fault zone, smooth joint bonds are used (Fig. 2*b*) to represent the fault core fractures that slip and dilate. Mechanical properties of the intact rock, damage zone, and the fault fractures are listed in Table 1.

Table 1. Mechanical properties of the intact rock, fault damage zone, and fault core fractures.

Parameter	Intact rock	Damage zone	Core fracture
Density (kg/m³)	2630	2630	—
Friction coefficient	0.9	0.9	0.9
Young's modulus (GPa)	50	30	—
Poisson's ratio	0.25	0.25	—
Tensile strength, mean ± stdev. (MPa)	9±6	2±0.5	1±0
Cohesion, mean ± stdev. (MPa)	25±7	5±1	5±0
Friction angle (°)	53	30	30
Dilation angle (°)	—	—	3
Normal stiffness (GPa/m)	—	—	300
Shear stiffness (GPa/m)	—	—	50

In situ stresses of 40 and 30 MPa are applied for the maximum and minimum horizontal stresses (SH and Sh), respectively. The set of in situ stresses is taken from Cornet et al. (2007, their eqs. 1*b* and 1*c*), assuming that the reservoir section is at depth z = 2000–2500 m, using

(7) $\mathrm{Sh} = 15.1 + 0.0179(z - 1458)$

(8) $\mathrm{SH} = 24.8 + 0.0198(z - 1458)$

The level of minimum horizontal stress applied in the model is comparable to that of Marcellus shale-gas plays in northeastern USA at 2000 m depths. According to Rutqvist et al (2013, 2015), the gradient of vertical stress (in this case the maximum principal stress) is 0.026 MPa/m. The minimum horizontal stress is set according to the ratio R = Sh/Sv = 0.6. Setting the depth to 2000 m, Sv = 52 MPa and Sh = 31 MPa. There is uncertainty in the ratio R.

Fig. 3. Applied rate of injection with time and total volume of fluid injected and two locations of injection, 200 and 400 m from the fault zone centre.

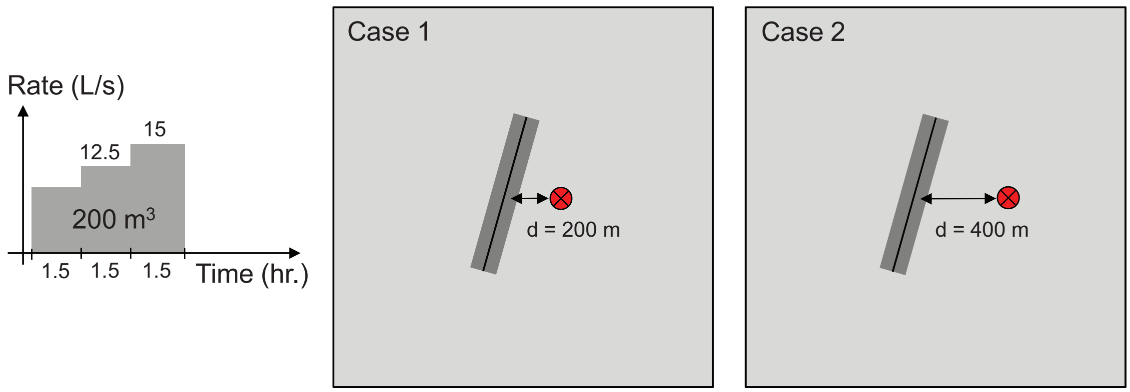

Fig. 4. Results of fluid injection at 200 m from the fault zone centre. Applied rate of injection is displayed by the gray bars (left), fluid pressure at the injection point by the blue curve (right), magnitudes of the induced invents by the red circles (right), and occurrence rate per minute of induced events by dark gray spikes (note: colours refer to the Web version of this paper).

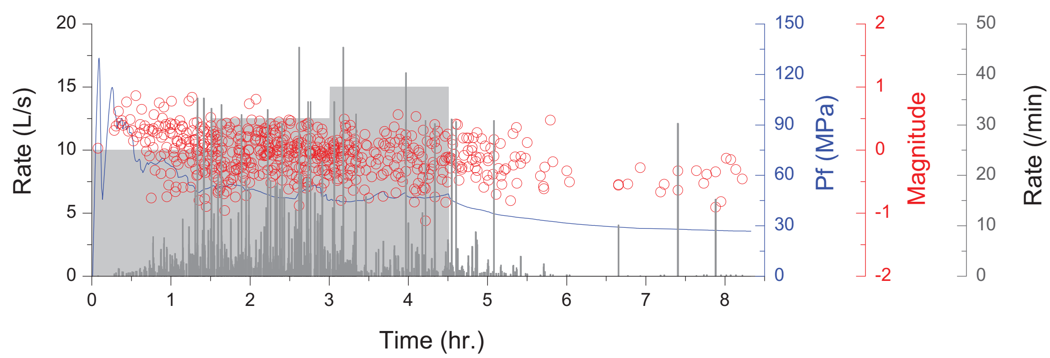

However, several sources, e.g., Cipolla et al. (2010), show a fracture closure stress of around 0.7 psi/ft (16 MPa/km), which corresponds to a ratio R = Sh/Sv = 0.6 (Rutqvist et al. 2015), justifying 30 MPa for the minimum horizontal stress.

Fluid injection is applied at 200 and 400 m distances from the fault zone centre at a constant rate, changing in three steps from 10 to 12.5 L/s then 15 L/s (Fig. 3). The total amount of volume of fluid injection is therefore 200 m^3. The amount of injected volume is far lower than what is often used in geothermal sites, i.e., >10 000 m^3 (McGarr 2014; Zang et al. 2014). However, it should be noted that the model is in two dimensions (2D) with a unit thickness of 1 m in the out-of-plane direction. Therefore, considering that the fluid injection is usually conducted along a few hundreds of metres in the open-hole section of a stimulation wellbore, the simulated volume of 200 m^3 is appropriate for a 1 m slice of the model. Assuming a 100 m long open-hole section, the effective fluid injection volume would be 20 000 m^3.

Numerical model results

Figure 4 shows the results of the case where the injection is applied at a 200 m distance from the fault zone centre. The figure contains applied rates of injection, fluid pressure monitored at the injection point, magnitudes of the induced events, and event occurrence rate. As indicated by the curve representing the fluid pressure at the injection point, the pressure drops after it reaches almost 120 MPa, where the fracture initiates. Fracture breakdown pressure (FBP) is estimated using

$$\text{FBP} = 3\text{Sh} - \text{SH} + T_0 \tag{9}$$

where Sh is the minimum horizontal stress (30 MPa), SH is the maximum horizontal stress (40 MPa), and T_0 is the tensile strength (9 ± 6 MPa). FBP is estimated to be between 53 and 65 MPa. The simulated FBP is far greater than estimated, because the estimated FBP is for a radial tensile fracture developing at the borehole wall and propagating bilaterally along the azimuth 0° and 180°, parallel to the orientation of the maximum horizontal stress (Zang and Stephansson 2010). However, in the reservoir model made by the bonded particle assembly, circular borehole geometry is not modeled and the fluid is injected into a void space surrounded by a few particles. As the fluid migration path is predefined by the particle arrangement, the fluid pressure should exceed the bond tensile strength plus the additional amount that should be given to induce fracture where the planes are not oriented parallel to the maximum horizontal stress.

The event occurrence rate is shown at the bottom of Fig. 4, which indicates that there is delay in the start of rate increase after the injection starts. This is due to the time taken to build up the fluid pressure level required to induce a fracture near the injection point. The occurrence rate is intense during the injection (mostly during second and third step rates), but significantly decreases in the post shut-in. However, high occurrence rates are noticed after the shut-in, in particular at 5 h and between 7 and 8 h. Figure 5 compares two sets of magnitudes: those of the induced events (left, computed by eqs. (4) and (6)) and those calculated from the cumulative slip of faults (right) derived from the average shear displacement of the fault core fractures, monitored at several selected times.

The curve shows that in the early stage of the injection (time: 0–1 h) the magnitudes of the induced events are generally higher than those determined from fault slip. However, during the time

Fig. 5. Magnitudes of the induced seismic events (left) and magnitudes associated with fault slip (right). The star represents the maximum magnitude observed in the KTB injection experiment (Zoback and Harjes 1997).

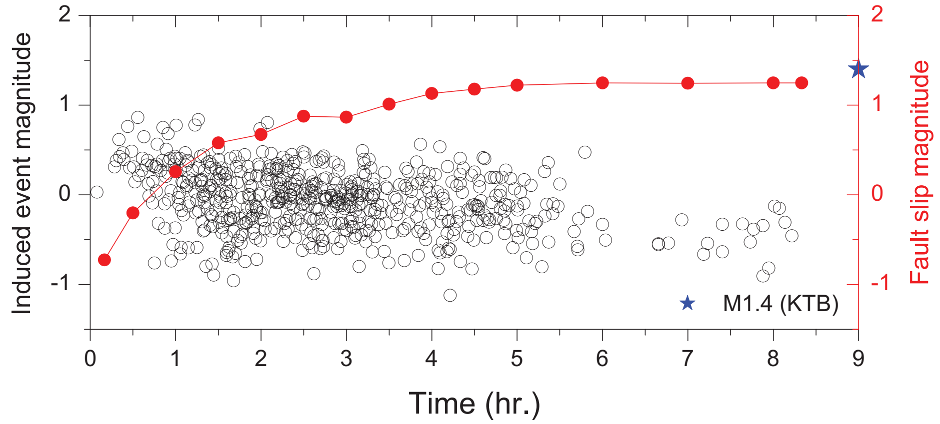

Fig. 6. Fluid pressure distribution at selected times: (*a*) 2.5 h, (*b*) 5 h, (*c*) 8.3 h.

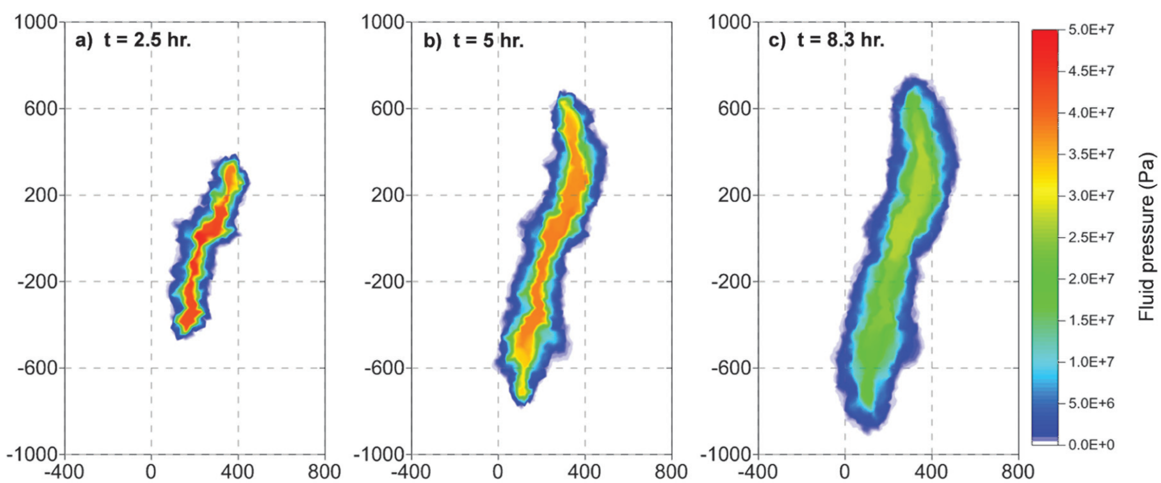

ranges between 1 and 2 h, a transition occurs where the magnitude from the fault slip exceeds the magnitudes of the induced events. After the shut-in, the intensity of the induced events decreases in terms of occurrence rate and magnitude as the injection pressure decreases.

As the model is in 2D, there should be an assumed fault plane area (A) to calculate the seismic moment M_0 using eq. (5). In this study, the fault plane area is 1500 m² (length 1500 m × width 1 m). For reference, the maximum magnitude event (M1.4) that is observed in the KTB injection experiment where the injection volume is the same as in the modeling, i.e., 200 m³, is shown by the star in Fig. 5.

Figure 6 shows the spatial distribution of the injected fluid pressure determined at three selected times: (*a*) t = 2.5 h, before shut-in; (*b*) t = 5 h, right after shut-in; and (*c*) t = 8.3 h, long after shut-in. The figure shows that fluid diffuses mostly in the direction of maximum horizontal stress and deviates slightly in the orientation of the fault zone (Fig. 6*a*). The speed of fluid diffusion is faster in the direction of maximum horizontal stress than that of minimum stress. From Figs. 6*b* and 6*c* it is seen that the area of high fluid pressure (>45 MPa), which is the upper limit of the sum of minimum horizontal stress and tensile strength, i.e., Sh + T_0 = 30 + 9 + 6 = 45 (shown in red, >45 MPa), decreases with time as the fluid diffuses to the surrounding rock mass.

Figure 7 shows the spatial and temporal distribution of the induced seismic events. The size of the events is scaled to their magnitude. Events are coloured according to their time of occurrence. To enhance the visibility, the pre shut-in events are coloured according to the time range of the applied rates of injection (red between 0 and 1.5 h, blue between 1.5 and 3 h, green between 3 and 4.5 h). The coordinates of the injection points are (400, 0) in Fig. 7*a* and (200, 0) in Fig. 7*b*. The figures show that most of the induced events are large in magnitude during the early stage of the injection (t < 4.5 h), and accompany a large number of seismic events in the fault damage zone. For the post shut-in events, events are coloured in grayscale, i.e., early events in light gray and late events in dark gray. Post shut-in induced events are mostly located at the tips of the seismicity cloud that is formed during the injection.

Figure 8 shows the evolution of the induced seismicity cloud and fluid pressure contour of 0.1 MPa evolving with time for the case of the injection 200 m from the fault zone centre. Two sets of seismicity are presented. The first set is marked by gray dots, showing seismic moments calculated using the moment tensor method (eqs. (3) and (4)). The second set is marked by red dots (in the Web version), displaying the seismic moments calculated as a function of displacement of the fault core fractures using eq. (5), and converted to moment magnitude using eq. (6). It is clear from the figure that magnitudes from the slip of the fault core fractures are lower than those from the induced events, which are mostly confined within the pressurized zone during the pre shut-in phase. However, the magnitudes from the slip of fault core fractures exceed the induced event magnitudes during the post

Fig. 7. Spatial and temporal distributions of the events induced by fluid injection at (*a*) 400 m and (*b*) 200 m distances from the fault zone centre. Sizes of events are scaled to the magnitude and coloured by the time of occurrence. Fluid pressure of 0.1 MPa is shown by the contour.

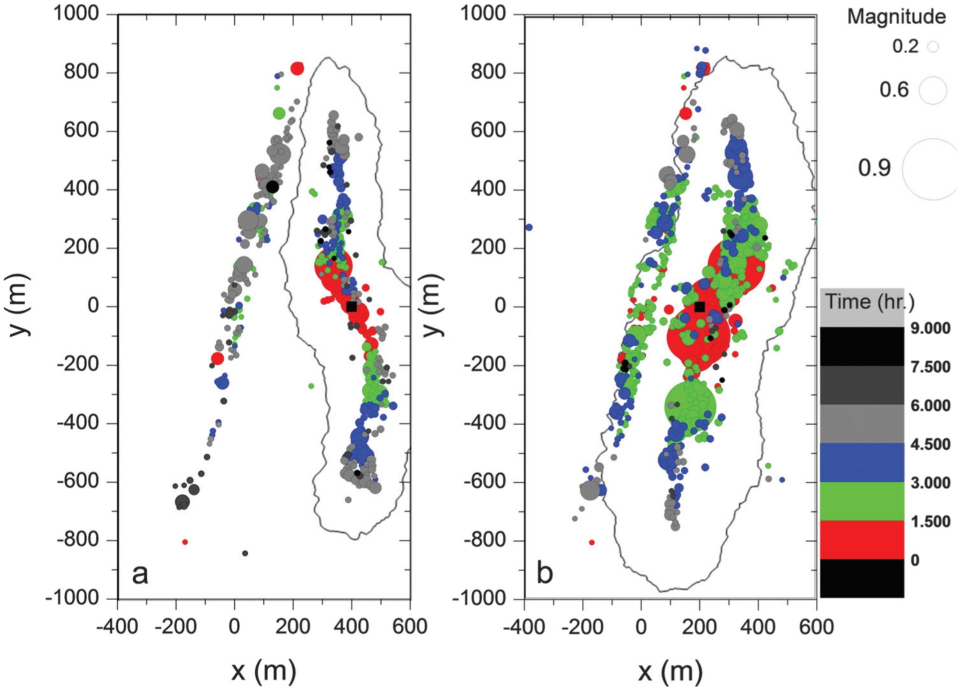

shut-in phase. This can be seen from the size of the fracture slip events and the induced events at a time of 5 h.

Discussion

It is seen in Fig. 5 that the magnitude calculated by the fault slip is almost constant after the shut-in. The slight increase in magnitude is due to the diffusion of the pressurized fluid into the fault zone, which reduces the frictional strength of the fault core fractures. The magnitude can show steady or abrupt increase when pre-existing joints are present around the fault zone depending on the density. As fracture zones can serve as fluid flow pathways where the pressurized fluid migrates into the fault zone, the fluid fills up the damage zones and consequently reduces the frictional strength. It is recommended to conduct a series of modeling cases where there are hundreds of metre-long joints with varying densities close to the fault zone. Results from such a model configuration might provide clues regarding the mechanisms of LMEs at some EGS sites, in particular where massive fluid injection is conducted near natural fault systems, e.g., Basel and St. Gallen EGS in Switzerland.

In Figs. 7 and 8, some of the post shut-in events are induced adjacent to the seismicity cloud that has formed during the injection, due to the diffusion of pressurized fluid. Fluid pressure of 0.1 MPa is indicated by the contour. The area inside the contour indicates where the fluid pressure exceeds 0.1 MPa. Many induced events within the fault zone are located outside of the fluid pressure contour, which means that these events occurred due to the fluid pressure falling below 0.1 MPa. However, considering that the tensile strength and cohesion of the damaged zone are 2 ± 0.5 and 5 ± 1 MPa, respectively, such low fluid pressure magnitudes may not effectively explain the events' occurrence. It is rather a combination of other factors, such as in situ stresses and fault movement caused by the expansion of the surrounding rock mass due to fluid injection. Therefore, these events are referred to not as "induced" but rather "triggered" by the fluid injection. This argument is consistent with that of McGarr and Simpson (1997), in that the term "induced" indicates a causative activity that accounts for most of the stress change or energy required to produce the earthquakes, whereas the term "triggered" describes a process that accounts for only a small fraction of the same stress change or energy.

Provided that the definitions of induced and triggered seismicity mentioned earlier are valid, it is seen in Figs. 7 and 8 that there are no triggered events on the left part of the fault zone, but there are several on the right part. This is mostly because injection is conducted in the right part, but it also may be attributed to the fault zone acting as a barrier that prevents the stress changes in the left side of the fault zone. Effective stress changes caused by the injection are mostly spent through fault movement and therefore the initial stress state in the left side of the fault zone is less altered.

Magnitude–frequency relations of the induced seismic events caused by fluid injection and events triggered by the slip of fault core fractures are compared in Fig. 9. Magnitude histograms (left) show that the range of magnitudes of the induced events is narrower than that of triggered events. The maximum magnitude of the induced events is smaller than that of the triggered events, which lowers the slope of the linear portion of the curve. The slope corresponds to the *b* parameter of the Gutenberg–Richter scaling law (Gutenberg and Richter 1954). The *b* parameters computed from the induced and triggered events are 2.34 and 0.99, respectively. The difference in *b*-values is consistent with Grünthal (2014), where the *b*-values of different types of induced seismic events and natural tectonic earthquakes are compared. Grünthal (2014) found that, in general, the induced seismicity *b*-value (1.94 ± 0.21) is among the highest of all types of induced seismic events and natural tectonic earthquakes (1.16 ± 0.05).

Moreover, Maxwell et al. (2009) and Downie et al. (2010) showed that the events recorded during hydraulic treatment have *b*-values close to 2, while the events associated with fault deformation have *b*-values close to 1. Analysis by Kratz et al. (2013) on the microseismic events associated with 13 horizontal wells in the Barnett shale in North Texas shows that the *b*-value of fracture-related events is close to 2 whereas the *b*-value of fault-related events is close to 1.

Many of the modeling results agree with some field observations in EGS sites, e.g., growth of seismicity clouds in the direction

Fig. 8. Temporal evolution of induced events (gray dots) and from fault core fractures caused by slip (red dots), and 0.1 MPa fluid pressure contour for the case of fluid injection at 200 m from the fault zone centre.

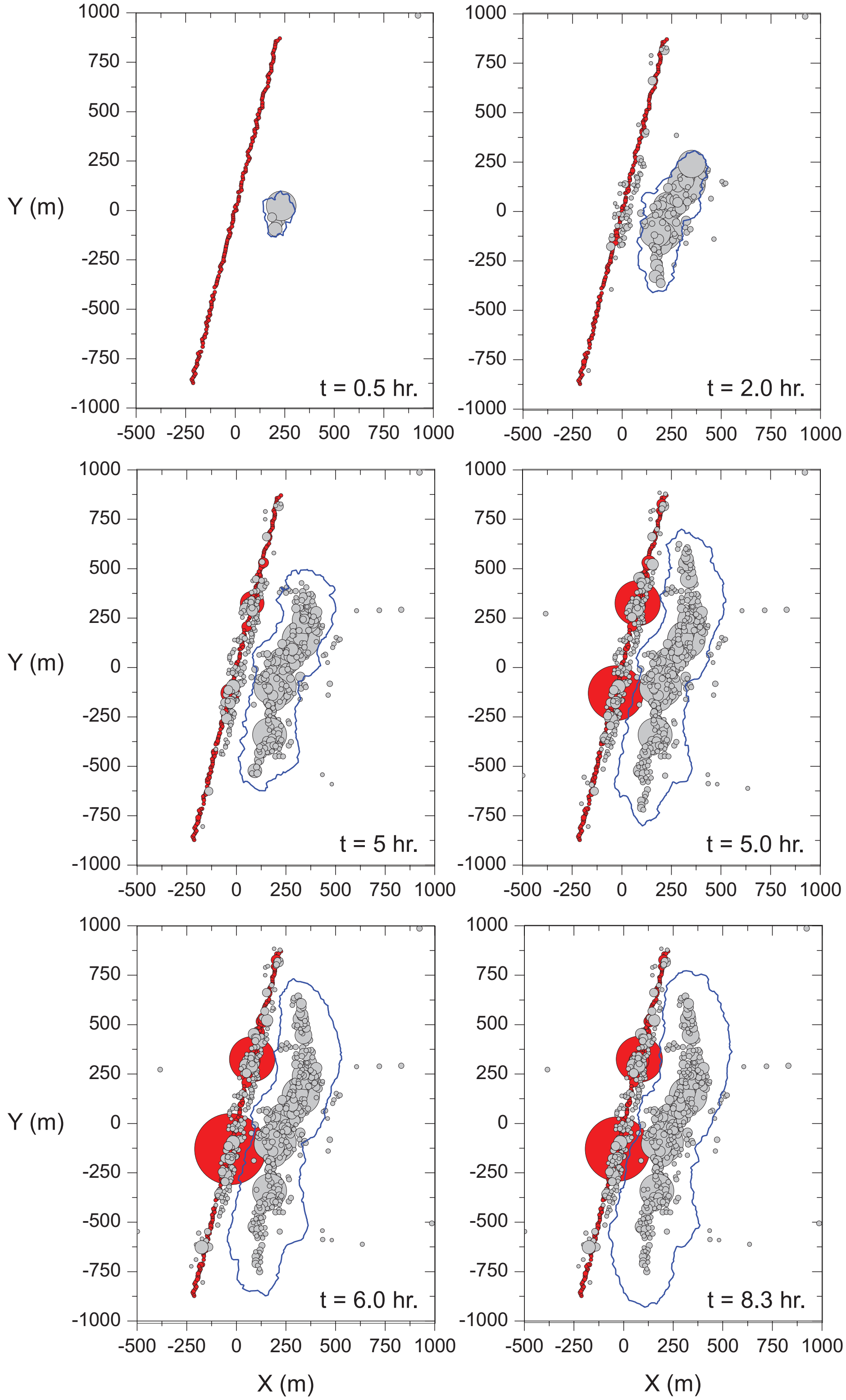

of maximum horizontal stress, smooth decay of fluid pressure at injection points in post shut-in, occurrence of post shut-in seismicity due to diffusion of fluid that is pressurized during injection, and larger magnitude earthquakes from the nearby fault slip in the post shut-in phase.

However, as the modeling is done in 2D to reproduce three-dimensional phenomena, the largest modeling uncertainty and limitation come from 2D simplification. In the 2D setting, it is difficult to estimate a representative injection rate and in particular there should be an assumed fault plane area to calculate the

Fig. 9. Magnitude histograms of the induced (red) and triggered (green) events and their cumulative frequency distributions (right) and calculated *b*-values.

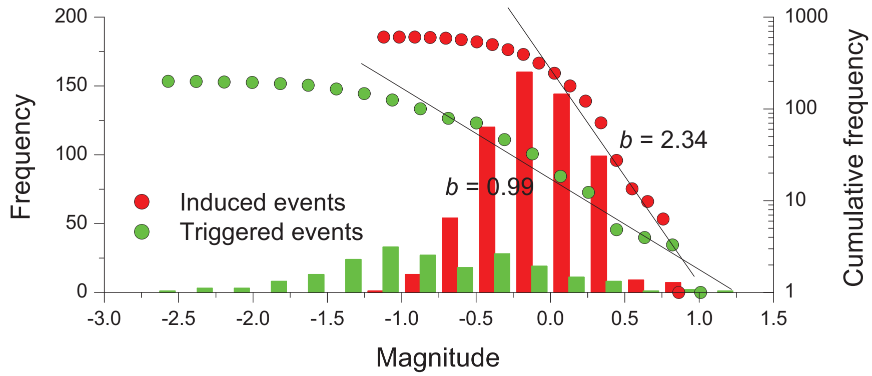

seismic moment M_0 (eq. (5)). In this study, the fault plane area is assumed to be 1500 m² (length 1500 m × width 1 m).

Particle size also affects earthquake magnitudes. If the particle diameters are set to a few centimetres, the resulting magnitude is far lower than the range of simulated seismic magnitudes in this study (–1~1). Having finer particles can be beneficial when precise modeling of fracture initiation and propagation in the borehole near-field is required. However, as the number of particles impacts the computation time–speed and efficiency, choosing a particle diameter range should be done with careful consideration of both model precision and computing efficiency. The particle diameter range 20–30 m used in this study is considered acceptable, as the resulting seismic magnitudes are between –1 and 2, which are comparable to the seismic events from shale-gas stimulations in the North America (Marcellus, Barnett, Eagle Ford, Woodford, Haynesville, Horn River; Warpinski (2009) and Warpinski et al. (2012)), and the seismic events from EGS operations in crystalline rock mass, e.g., Basel (Mukuhira et al. 2013) and Soultz (Baisch et al. 2010).

Conclusions

This study investigates fluid injection, induced seismicity, and triggered seismicity in a fault zone adjacent to fluid injection using discrete element modeling. The numerical results indicate that fluid injection triggers seismic events in a nearby fault zone. The level of influence diminishes with increasing distance from the injection location to the fault zone. Seismic events in the fault zone are triggered rather than induced as they are located far outside of the fluid pressure contour of 0.1 MPa. This implies that small perturbations of the fluid pressure (<0.1 MPa) trigger those events, which are located in a fault zone, critically oriented and stressed under a given stress field.

In the early stage of fluid injection, magnitudes of the induced events are relatively larger than those of events in the fault zone triggered by fluid injection. However, a transition takes place where the seismic magnitude associated with the fault slip becomes larger than the magnitude of the induced events. Magnitudes and rates of the induced events decrease in the post shut-in phase, whereas the magnitudes of events from the fault slip increase slowly due to continuous migration of fluid into the fault zone, which consequently reduces the frictional strength and causes further slip.

The magnitude range of the induced events is narrower than that of events of the fault fracture slip that was triggered by fluid injection. The maximum magnitude of the induced events is smaller than the maximum magnitude of the fault fracture slip events, making the slope of the magnitude–frequency distribution of the induced events larger than that of the triggered events.

The modeling results show fair agreement with field observations at some EGS sites. Better understanding of the fault behaviour by nearby fluid injection and its implication on controlling induced seismicity and mitigation of larger magnitude events can be achieved by conducting more simulation runs with varying geological conditions and operational parameters, e.g., cyclic rate injection as was done by Zang et al. (2013) and Yoon et al. (2015*a*, 2015*b*).

Acknowledgements

This work was financially supported by the German Federal Ministry for Economic Affairs and Energy (BMWi) under grant 0325451C. This work was also supported by the Renewable Energy Core Technology Program of the Korean Institute of Energy Technology Evaluation and Planning (KETEP) through a grant funded by the Ministry of Trade, Industry & Energy of Republic of Korea (No. 20133030000240).

References

Al-Busaidi, A., Hazzard, J.F., and Young, R.P. 2005. Distinct element modeling of hydraulically fractured Lac du Bonnet granite. Journal of Geophysical Research, **110**: B06302. doi:10.1029/2004JB003297.

Baisch, S., Vörös, R., Rothert, E., Stang, H., Jung, R., and Schellschmidt, R. 2010. A numerical model for fluid injection induced seismicity at Soultz-sous-Forêts. International Journal of Rock Mechanics and Mining Sciences, **47**: 405–413. doi:10.1016/j.ijrmms.2009.10.001.

Cipolla, C.L., Lolon, E.P., Erdle, J.C., and Rubin, B. 2010. Reservoir modeling in shale-gas reservoirs. Society of Petroleum Engineers SPE Reservoir Evaluation & Engineering, **13**: SPE-125530-PA. doi:10.2118/125530-PA.

Cornet, F.H., Bérard, Th, and Bourouis, S. 2007. How close to failure is a granite rock mass at a 5 km depth? International Journal of Rock Mechanics and Mining Sciences, **44**: 47–66. doi:10.1016/j.ijrmms.2006.04.008.

de Pater, C.J., and Baisch, S. 2011. Geomechanical study of Bowland shale seismicity. Synthesis Report, November 2011, Cuadrilla Resources Ltd., U.K.

Diehl, T., Kraft, T., Eduard, K., Nicholas, D., Clinton, J., and Wiemer, S. 2014. High-precision relocation of induced seismicity in the geothermal system below St. Gallen (Switzerland). Geophysical Research Abstracts, **16**: EGU2014-12541-1.

Downie, R.C., Kronenberger, E., and Maxwell, S.C. 2010. Using microseismic source parameters to evaluate the influence of faults on fracture treatments - a geophysical approach to interpretation. Presented at the Society of Petroleum Engineers Conference, Florence, Italy, 19–22 September. SPE 134772.

Grünthal, G. 2014. Induced seismicity related to geothermal projects versus natural tectonic earthquakes and other types of induced seismic events in Central Europe. Geothermics, **52**: 22–35. doi:10.1016/j.geothermics.2013.09.009.

Gutenberg, B., and Richter, C. 1954. Seismicity in the earth. 2nd ed. Princeton University Press, Princeton, N.J. pp. 16–25.

Hanks, T.C., and Kanamori, H. 1979. A moment magnitude scale. Journal of Geophysical Research, **84**: 2348–2350. doi:10.1029/JB084iB05p02348.

Häring, M.O., Schanz, U., Ladner, F., and Dyer, B.C. 2008. Characterisation of Basel 1 enhanced geothermal system. Geothermics, **37**: 469–495. doi:10.1016/j.geothermics.2008.06.002.

Hazzard, J.F., and Young, R.P. 2002. Moment tensors and micromechanical models. Tectonophysics, **356**: 181–197. doi:10.1016/S0040-1951(02)00384-0.

Hazzard, J.F., Young, R.P., and Oates, S.J. 2002. Numerical modeling of seismicity induced by fluid injection in a fractured reservoir. *In* Mining and Tunnel Innovation and Opportunity, Proceedings of the 5th North American Rock Mechanics Symposium, Toronto, Ont. pp. 1023–1030.

Hökmark, H., Lönnqvist, M., and Fälth, B. 2010. THM-issues in repository rock – Thermal, mechanical, thermo-mechanical and hydro-mechanical evolution of the rock at the Forsmark and Laxemar sites. SKB – Swedish Nuclear Fuel and Waste Management Co. Technical Report TR-10-23.

ICG. 2008. PFC2D (Particle Flow Code in 2 Dimensions). Version 4.0. Itasca Consulting Group Inc. (ICG), Minneapolis, Minn.

Kraft, T., Mai, P.M., Wiemer, S., Deichmann, N., Ripperger, J., Kästli, P., Bachmann, C., Fäh, D., Wössner, J., and Giardini, D. 2009. Enhanced geothermal systems: mitigating risk in urban areas. Eos, **90**(32): 273–274. doi:10.1029/2009EO320001.

Kratz, M., Aulia, A., and Hill, A. 2013. Identifying fault activation in shale reservoirs using microseismic monitoring during hydraulic stimulation: source mechanisms, *b* values, and energy release rates. Geohorizons, July 2013/19.

Maxwell, S.C., Jones, M., Parker, R., Miong, S., Leaney, S., Dorval, D., D'Amico, D., Logel, J., Anderson, E., and Hammermaster, K. 2009. Fault activation during hydraulic fracturing. Society of Exploration Geophysicists, Expanded Abstracts 2009. pp. 1552–1556. doi:10.1190/1.3255145.

Mazzoldi, A., Rinaldi, AP, Borgia, A, and Rutqvist, J. 2012. Induced seismicity within geological carbon sequestration projects: maximum earthquake magnitude and leakage potential from undetected faults. International Journal of Greenhouse Gas Control, **10**: 434–442. doi:10.1016/j.ijggc.2012.07.012.

McGarr, A. 2014. Maximum magnitude earthquakes by fluid injection. Journal of Geophysical Research Solid Earth, **119**: 1008–1019. doi:10.1002/2013JB010597.

McGarr, A., and Simpson, DW. 1997. A broad look at induced and triggered seismicity. *In* Rockbursts and seismicity in mines, Proceedings of the 4th International Symposium on Rockbursts and Seismicity in Mines. *Edited by* S.J. Gilbowicz and S. Lasocki. A.A. Balkema, Rotterdam, the Netherlands. pp. 385–396.

Mukuhira, Y., Asanuma, H., Niitsuma, H., and Häring, M.O. 2013. Characteristics of large-magnitude microseismic events recorded during and after stimulation of a geothermal reservoir at Basel, Switzerland. Geothermics, **45**: 1–17. doi:10.1016/j.geothermics.2012.07.005.

Munier, R., and Hökmark, H. 2004. Respect distances. Rationale and means of computation. SKB – Swedish Nuclear Fuel and Waste Managements Co. Technical Report R-04-17.

Rutqvist, J., Rinaldi, A.P., Cappa, F., and Moridis, G.J. 2013. Modeling of fault reactivation and induced seismicity during hydraulic fracturing of shale-gas reservoirs. Journal of Petroleum Science and Engineering, **107**: 31–44. doi:10.1016/j.petrol.2013.04.023.

Rutqvist, J., Rinaldi, A.P., Cappa, F., and Moridis, G.J. 2015. Modeling of fault activation and seismicity by injection directly into a fault zone associated with hydraulic fracturing of shale-gas reservoirs. Journal of Petroleum Science and Engineering, **127**: 377–386. doi:10.1016/j.petrol.2015.01.019.

Warpinski, N.R. 2009. Microseismic monitoring: inside and out. Journal of Petroleum Technology, **61**(11): 80–85. [Document ID: SPE-118537-JPT] doi:dx.doi.org/10.2118/118537-JPT.

Warpinski, N.R., Mayerhofer, M.J., Agarwal, K., and Du, J. 2012. Hydraulic fracture geomechanics and microseismic source mechanisms. SPE Journal, **8**(4): 766–780. [Document ID: SPE-159835-PA]. doi:10.2118/158935-PA.

Yoon, J.S., Zang, A., and Stephansson, O. 2012. Simulating fracture and friction of Aue granite under confined asymmetric compressive test using clumped particle model. International Journal of Rock Mechanics and Mining Sciences, **49**: 68–83. doi:10.1016/j.ijrmms.2011.11.004.

Yoon, J.S., Zang, A., and Stephansson, O. 2013. Simulation of hydraulic stimulation of fractured reservoir and induced seismicity using discrete element-fracture network model. *In* Proceedings of the Thirty-Eighth Workshop on Geothermal Reservoir Engineering, Stanford, Calif., 11–13 February 2013. SGP-TR-198.

Yoon, J.S., Zang, A., and Stephansson, O. 2014. Numerical investigation on optimized stimulation of intact and naturally fractured deep geothermal reservoirs using hydro-mechanical coupled discrete particles joints model. Geothermics, **52**: 165–184. doi:10.1016/j.geothermics.2014.01.009.

Yoon, J.S., Zimmermann, G., and Zang, A. 2015*a*. Discrete element modeling of cyclic rate fluid injection at multiple locations in naturally fractured reservoirs. International Journal of Rock Mechanics and Mining Sciences, **74**: 15–23. doi:10.1016/j.ijrmms.2014.12.003.

Yoon, J.S., Zimmermann, G., and Zang, A. 2015*b*. Numerical investigation of stress shadowing in fluid injection-induced fracture propagation in naturally fractured geothermal reservoirs. Rock Mechanics & Rock Engineering, **48**(4): 1439–1454. doi:10.1007/s00603-014-0695-5.

Zang, A., and Stephansson, O. 2010. Stress field of the earth's crust. Springer Science + Business Media B.V., Dordrecht.

Zang, A., Yoon, J.S., Stephansson, O., and Heidbach, O. 2013. Fatigue hydraulic fracturing by cyclic reservoir treatment enhances permeability and reduces induced seismicity. Geophysical Journal International, **195**: 1282–1287. doi:10.1093/gji/ggt301.

Zang, A., Oye, V., Jousset, P., Deichmann, N., Gritto, R., McGarr, A., Majer, E., and Bruhn, D. 2014. Analysis of induced seismicity in geothermal reservoirs – an overview. Geothermics, **52**: 6–21. doi:10.1016/j.geothermics.2014.06.005.

Zhao, X., and Young, R.P. 2011. Numerical modeling of seismicity induced by fluid injection in naturally fractured reservoirs. Geophysics, **76**(6): WC167–WC180. doi:10.1190/geo2011-0025.1.

Zoback, M.D., and Harjes, H.-P. 1997. Injection-induced earthquakes and crustal stress at 9 km depth at the KTB deep drilling site, Germany. Journal of Geophysical Research, **102**: 18477–18491. doi:10.1029/96JB02814.